ACS Infectious Diseases

pubs.acs.org/journal/aidcbc Article

A Potent Host Defense Peptide Triggers DNA Damage and Is Active against Multidrug-Resistant Gram-Negative Pathogens

Samuel A. Juliano, Leonardo F. Serafim, Searle S. Duay, Maria Heredia Chavez, Gaurav Sharma, Mary Rooney, Fatih Comert, Scott Pierce, Andrei Radulescu, Myriam L. Cotten, Mihaela Mihailescu, Eric R. May, Alexander I. Greenwood, Rajeev Prabhakar,* and Alfredo M. Angeles-Boza*

Cite This: *ACS Infect. Dis.* 2020, 6, 1250−1263 Read Online

ACCESS | Metrics & More | Article Recommendations | Supporting Information

ABSTRACT: Gram-negative bacteria are some of the biggest threats to public health due to a large prevalence of antibiotic resistance. The difficulty in treating bacterial infections, stemming from their double membrane structure combined with efflux pumps in the outer membrane, has resulted in a much greater need for antimicrobials with activity against these pathogens. Tunicate host defense peptide (HDP), Clavanin A, is capable of not only inhibiting Gram-negative growth but also potentiating activity in the presence of Zn(II). Here, we provide evidence that the improvements of Clavanin A activity in the presence of Zn(II) are due to its novel mechanism of action. We employed *E. coli* TD172 (Δ*recA::kan*) and the terminal deoxynucleotidyl transferase dUTP nick end labeling (TUNEL) assay to show *in cellulae* that DNA damage occurs upon treatment with Clavanin A. *In vitro* assays demonstrated that Zn(II) ions are required for the nuclease activity of the peptide. The quantum mechanics/molecular mechanics (QM/MM) calculations were used to investigate the mechanism of DNA damage. In the rate-determining step of the proposed mechanism, due to its Lewis acidity, the Zn(II) ion activates the scissile P−O bond of DNA and creates a hydroxyl nucleophile from a water molecule. A subsequent attack by this group to the electrophilic phosphorus cleaves the scissile phosphoester bond. Additionally, we utilized bacterial cytological profiling (BCP), circular dichroism (CD) spectroscopy in the presence of lipid vesicles, and surface plasmon resonance combined with electrical impedance spectroscopy in order to address the apparent discrepancies between our results and the previous studies regarding the mechanism of action of Clavanin A. Finally, our approach may lead to the identification of additional Clavanin A like HDPs and promote the development of antimicrobial peptide based therapeutics.

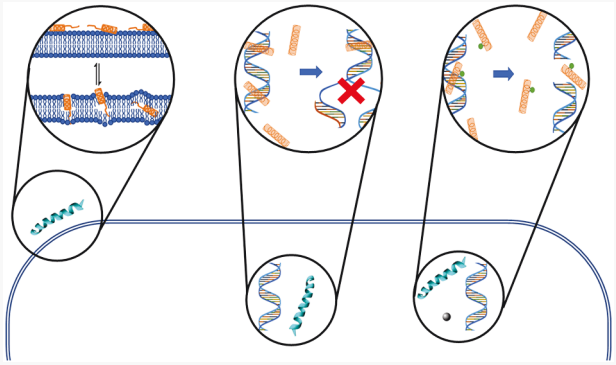

KEYWORDS: *DNA damage, multidrug resistance, Gram-negative pathogens, host defense peptide*

The worldwide emergence of antibiotic-resistant bacteria has endangered the efficacy of antibiotics. Some frightening projections estimate that antibiotic-resistant bacteria will result in the death of 2.4 million people annually by 2050, costing in excess of $3 billion per year.[1] Hospital acquired infections are responsible for the death of over 1 million patients per year in the US alone, with the primary offenders including the so-called ESKAPE (*Enterococcus faecium*, *Staphylococcus aureus*, *Klebsiella pneumoniae*, *Acinetobacter baumannii*, *Pseudomonas aeruginosa*, and *Enterobacter* species) pathogens.[2,3] Isolates of each of these bacterial species have been reported to contain multiple mechanisms for antibiotic resistance, setting the stage for the fulfilment of these projections.[4] Gram-negative bacteria, in particular, have shown an alarming prevalence of antibiotic resistance. For example, particular species of *Acinetobacter* and *Pseudomonas* are showing resistance to all available antibiotics, and carbapenem resistance genes from *Klebsiella* spp. have spread to Gram-negative bacteria worldwide.[5,6] With so many bacteria showing resistance, even to some of the antibiotics of last resort, the need for novel therapeutic compounds to combat the problem is greater than ever.

In recent years, host defense peptides (HDPs) have elicited great interest as tools to supplement our antibiotic arsenal. Their advantages include broad spectrum activity and low incidence of resistance development. Clavanin A (ClavA, VFQFLGKIIHHVGNFVHGFSHVF−NH_2), a 23-residue HDP isolated from the hemocytes of the solitary tunicate

Received: February 4, 2020
Published: April 6, 2020

https://dx.doi.org/10.1021/acsinfecdis.0c00051
ACS Infect. Dis. 2020, 6, 1250−1263

Styela clava, has shown great promise as a novel therapeutic against a wide range of bacterial pathogens. *In vitro* studies of murine wound infection models showed improved healing and eradication of bacteria, while in systemic infection models, ClavA treatment resulted in increased survival for both *Escherichia coli* and *Staphylococcus aureus* infected mice.[7] In addition to this, ClavA has also been proven to be effective against biofilms, preventing the formation of *E. coli* and *S. aureus* biofilms and perturbing preformed biofilms of *K. pneumoniae*.[8]

In our previous studies of ClavA, we found evidence for a Zn(II)-regulated intracellular mechanism of action (MoA), which we hypothesized to involve damage to bacterial DNA.[9] This hypothesis was supported by evidence of *in vitro* DNA cleavage by ClavA−Zn(II) and inhibition of ClavA activity in *E. coli* strains lacking the ability to transport Zn(II) ions. These results represent a novel MoA for zinc-binding HDPs. This remarkable finding was surprising as previous studies from three different laboratories suggested that ClavA exerts its activity by permeabilizing the inner and outer membranes of Gram-negative bacteria in a stepwise manner.[10−12] Lehrer and co-workers, who first isolated the Clavanin family, were able to demonstrate a pH-dependent MoA for ClavA with the peptide showing greater activity at lower pH values. This idea was later expanded upon by van Kan et al., who proposed two mechanisms for ClavA acting at different pH values.[10,13] At neutral pH (7.4), it was concluded that the MoA of ClavA involves nonspecific pore formation driven by hydrophobic effects, while at low pH (5.5), the activity was hypothesized to originate from increased permeability of the membrane to small ions, likely the result of the interaction between ClavA and a membrane ionophore or ATP synthase.[13]

Zinc, the second most abundant trace metal in human cells after iron, is an important micronutrient for many cellular processes in mammalian cells, including DNA and RNA synthesis, metabolism, and membrane stabilization.[14−16] More importantly, zinc(II) deficiencies have been found to be important in several chronic diseases, including diabetes and neurodegenerative diseases, as well as increase susceptibility to many infectious diseases, including HIV, malaria, and bacterial infections.[17] Important immune functions, such as phagocytosis and intracellular killing, are affected by zinc deficiency.[18] Zinc(II) ions are a common weapon used by eukaryotes to combat bacteria. For example, zinc levels in blood serum of infected mice can reach up to 900 μM.[19] Zinc is also trafficked into the phagosome of murine macrophages infected with mycobacteria. When infected with *Mycobacterium tuberculosis*, phagosomal zinc concentrations reach up to 459 μM after 24 h post-infection.[20] Although the concentration of zinc ions reaches very high micromolar levels, even higher concentrations seem to be needed for it to have a bactericidal effect. Zinc concentrations of 1 mM have been shown to abolish the growth of wild-type *Streptococcus pneumoniae*, while 250 μM Zn(II) only delays its growth. In *S. clava* hemolymph, the zinc concentration was found to be 26.7 ± 7.1 μM, though it is likely that the local concentration within phagocytic cells is much higher.[9] Additionally, several HDPs have been shown to require Zn(II) ions as important cofactors to their antimicrobial activities.[20] The study of the synergy between ClavA and Zn(II) could lead to a better understanding of these systems.

In order to further understand the Zn(II) based DNA cleavage mechanism and to illuminate the apparent disparity in mechanisms of action for ClavA, we utilize a number of chemical, biological, and computational methods. Altogether, we were able to not only present a computationally derived mechanism of ClavA−Zn(II) DNA cleavage but also propose an explanation for the various reported mechanisms of action ascribed to ClavA.

RESULTS

Zn(II) Potentiates the Antimicrobial Activity of ClavA against Gram-Negative Pathogens. We have previously shown that, when ClavA is combined with Zn(II), the activity of the peptide against *E. coli* is increased. In order to determine if this activity potentiation is unique to *E. coli*, we tested the activity of ClavA and ClavA−Zn(II) against the Gram-negative ESKAPE pathogens, including some multidrug-resistant clinical isolates. Gram-negative pathogens are of great interest due to the difficulty of penetrating their double membrane structure, with the outer membrane containing lipopolysaccharide (LPS) and lipid A, which aid in defending the bacteria against cationic AMPs.[21,22] Additionally, Gram-negative bacteria contain efflux pumps that remove not only small molecules from the cytoplasm and periplasm but also many AMPs. The results of testing ClavA and ClavA−Zn(II) against Gram-negative bacteria are summarized in Table 1. In every case, we observed a decrease in the minimum inhibitory concentration (MIC) upon incubation of the peptide with Zn(II) at double the peptide concentration, which correlates to an increase in activity. Importantly, this improvement in activity is also seen in multidrug-resistant ESKAPE pathogen clinical isolates and multidrug-resistant *E. coli*, though the Zn(II) based potentiation against *E. coli* AR Bank #0114 is not quite as pronounced as for the wild-type *E. coli*.[23] The activity of ClavA against *P. aeruginosa* and *K. pneumoniae* was above the limit of detection of the experiment, so they can only be said to show at least 8- and 4-fold improvements, respectively, while activity against *A. baumannii* and *Enterobacter cloacae* each improved 4-fold upon the addition of Zn(II). While none of these quite reached the 16-fold improvement seen against *E. coli*, the activity potentiation observed is still very promising for the effectiveness of ClavA−Zn(II) against other Gram-negative pathogens. Additionally, the fact that ClavA−Zn(II) showed improvement against multidrug-resistant clinical

Table 1. Clavanin A Minimum Inhibitory Concentrations against Various Wild-Type and Drug-Resistant Bacteria

bacterial strain	ClavA MIC (μM)	ClavA−Zn(II) MIC (μM)	fold increase in ClavA activity	Zn(II) MIC (μM)
E. coli MG1655[a]	64	4	16-fold	1024
E. coli TD172	8	2	4-fold	4096
E. coli AR Bank #0114[b]	64	8	8-fold	2048
K. pneumoniae AR Bank #0113[b]	>256	128	≥4-fold	8192
A. baumannii Naval-17[b]	32	8	4-fold	1024
P. aeruginosa PA01	>256	64	≥8-fold	2048
P. aeruginosa AR Bank #0229[b]	>256	64	≥8-fold	2048
E. cloacae AR Bank #0136[b]	256	64	4-fold	2048

[a]Taken from ref 9. [b]Multidrug-resistant clinical isolate. Zinc ion concentrations are 2 times that of the peptide.

https://dx.doi.org/10.1021/acsinfecdis.0c00051
ACS Infect. Dis. 2020, 6, 1250−1263

isolates provides further evidence of how effective ClavA is as an antimicrobial compound.

These results indicate a strong synergy between ClavA and zinc ions when coupled with the MIC values for Zn(II) against these pathogens (Table S1). The lowest MIC recorded for Zn(II) was 1 mM against *E. coli* MG1655 and *A. baumannii* Naval-17, which is still double the highest zinc concentration used in any of the ClavA−Zn(II) MIC measurements. In many cases, the MIC of Zn(II) with ClavA is a full order of magnitude lower than the MIC of Zn(II) alone. This improvement in activity clearly indicates strong synergism between ClavA and Zn(II) ions.

Clavanin A Shows Nuclease Activity *In Cellulae*. Although we have shown evidence that ClavA−Zn(II) can damage DNA in an *in vitro* assay,[9] proof of this damage *in cellulae* is absent. In order to prove that this activity occurs within living bacteria, we employed *E. coli* TD172 (Δ*recA::kan*) in which the gene for the DNA repair protein RecA has been deleted. Treatments that lead to DNA damage will thus be more potent as the Δ*recA* strain is less capable of repairing the damage. Both ClavA and ClavA−Zn(II) show improved activities against *E. coli* TD172 as compared with wild-type *E. coli* (Table 1), though the 2-fold increase in activity for ClavA−Zn(II) does not represent a significant change. It is likely that the range of 2−4 μM represents the absolute minimum amount of ClavA−Zn(II) required to inhibit growth through DNA cleavage. The fact that both ClavA and ClavA−Zn(II) approach this minimum amount in the ΔrecA *E. coli* provides more concrete evidence that DNA damage is important to the activity of ClavA.

While MICs against *E. coli* TD172 provide evidence that *E. coli* that are incapable of repairing DNA damage are more susceptible to ClavA and ClavA−Zn(II), these results do not definitively prove that DNA damage is occurring, nor can they quantify the amount of damage. With that aim in mind, we employed the terminal deoxynucleotidyl transferase dUTP nick end labeling (TUNEL) assay, which fluorescently labels strand breaks to allow for quantification. As can be seen in Figure 1, the DNA damage caused by ClavA−Zn(II) is steady

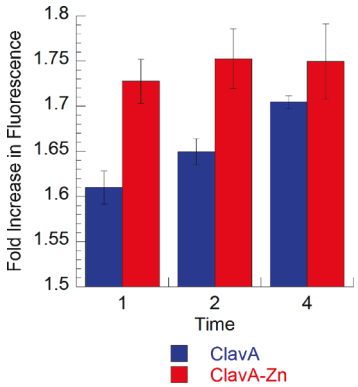

Figure 1. TUNEL assay results for ClavA and ClavA−Zn showing the fold increase in DNA damage over the untreated control.

across all time points at about 75% higher than baseline, whereas ClavA alone takes more time to reach the same level, with the two showing statistically identical levels of damage after 4 h. It is likely that ClavA−Zn(II) is causing immediate DNA damage due to the abundance of Zn(II) ions available for binding, while ClavA alone takes longer to achieve statistically similar levels due to the need to scavenge zinc ions from the *E. coli* themselves. These results provide proof that the ClavA−Zn(II) complex is capable of damaging DNA in intact bacterial cells.

In addition to the results obtained from the TUNEL assay, we were also able to use DNA damage to provide further evidence for the conclusion that His17 and His21 are responsible for the Zn(II) based activity of ClavA. The results of an *in vitro* DNA cleavage assay using ClavA−H17A and ClavA−H21A (Figure S1) show that there is no DNA cleavage in the presence of Zn(II) when either of the proposed histidine residues is absent from the sequence.

Further evidence for DNA as the target of ClavA−Zn(II) can be observed in the MIC values obtained using all the D-amino acid forms of ClavA. The MICs observed for D-ClavA and D-ClavA−Zn(II) against *E. coli* MG1655 were both found to be 32 μM, showing none of the potentiation usually observed for the zinc-containing peptide. Often, HDPs with achiral targets, such as the membrane, will show a minimal change in MIC when D-amino acids are used, whereas those with chiral targets, like DNA, will see diminished activity.[24−27] The change in MIC from 4 to 32 μM for ClavA−Zn(II) is indicative of a peptide with a chiral target, further promoting the likelihood of DNA as the target molecule.

Quantum Mechanics/Molecular Mechanics (QM/MM) Calculations Allow for the Determination of the Nuclease Mechanism of ClavA−Zn(II). The electrostatic surface potential and helical wheel projection of ClavA displaying its amphipathic character are shown in Figure S2. In the α-helical conformation, the hydrophilic and lipophilic residues are located on opposite sides of the peptide. Every pose provided by molecular docking shows that the positively charged hydrophilic side of ClavA binds to the negatively charged major groove of DNA, while the hydrophobic side of ClavA is exposed to the water solvent. In the lowest energy docked pose, ClavA occupies the major groove of DNA and interacts through multiple hydrogen bonds and CH−π interactions and Zn(II) ion is located ∼8 Å away from the closest phosphate group of DNA. During the MD simulations using this pose, the Zn(II) ion rapidly approaches the phosphate group of DNA and binds the negatively charged oxygen atom in a monodentate fashion. In the equilibrated structure, residues Lys7, His10, His11, Asn14, His17, and Ser 20 of ClavA are responsible for retaining its position in the major groove of DNA through hydrogen bonding with phosphate groups, while His10 and His17 associate through CH−π interactions with cytosine base pairs. These interactions also help to maintain the α-helicity of the fragment of ClavA that is inserted in the major groove of DNA. The small root-mean-square-fluctuations (RMSFs) support the overall stability of the α-helical structure of ClavA (Figures S2 and S3).

In the most representative structure derived from the MD simulations, the Zn(II) ion is found to interact with His17, His21, a phosphate group (in the monodentate form), and three solvent water molecules (Figure 2).

This structure was subsequently utilized to investigate the mechanism of DNA hydrolysis by ClavA through a hybrid two-layer (QM/MM) ONIOM approach.[28−30] In the mechanism, the Zn(II) ion is proposed to be involved in the Lewis acid activation, nucleophile activation, and generation of a good leaving group.[31−35] In the optimized structure of the reactant (**R**), Zn(II) is coordinated to two histidine residues (His17 and His21), one hydroxyl ion (−OH), a water molecule, and a

https://dx.doi.org/10.1021/acsinfecdis.0c00051
ACS Infect. Dis. 2020, 6, 1250−1263

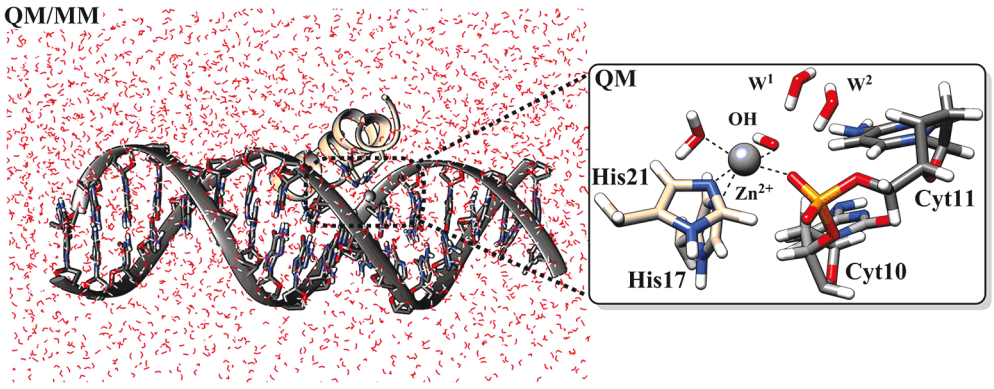

Figure 2. MD equilibrated structure of the ClavA−Zn(II) complex used for the QM/MM (ONIOM) calculations. Some hydrogen atoms and solvent water molecules were omitted for clarity. Nitrogen in blue, phosphorus in orange, and oxygen in red.

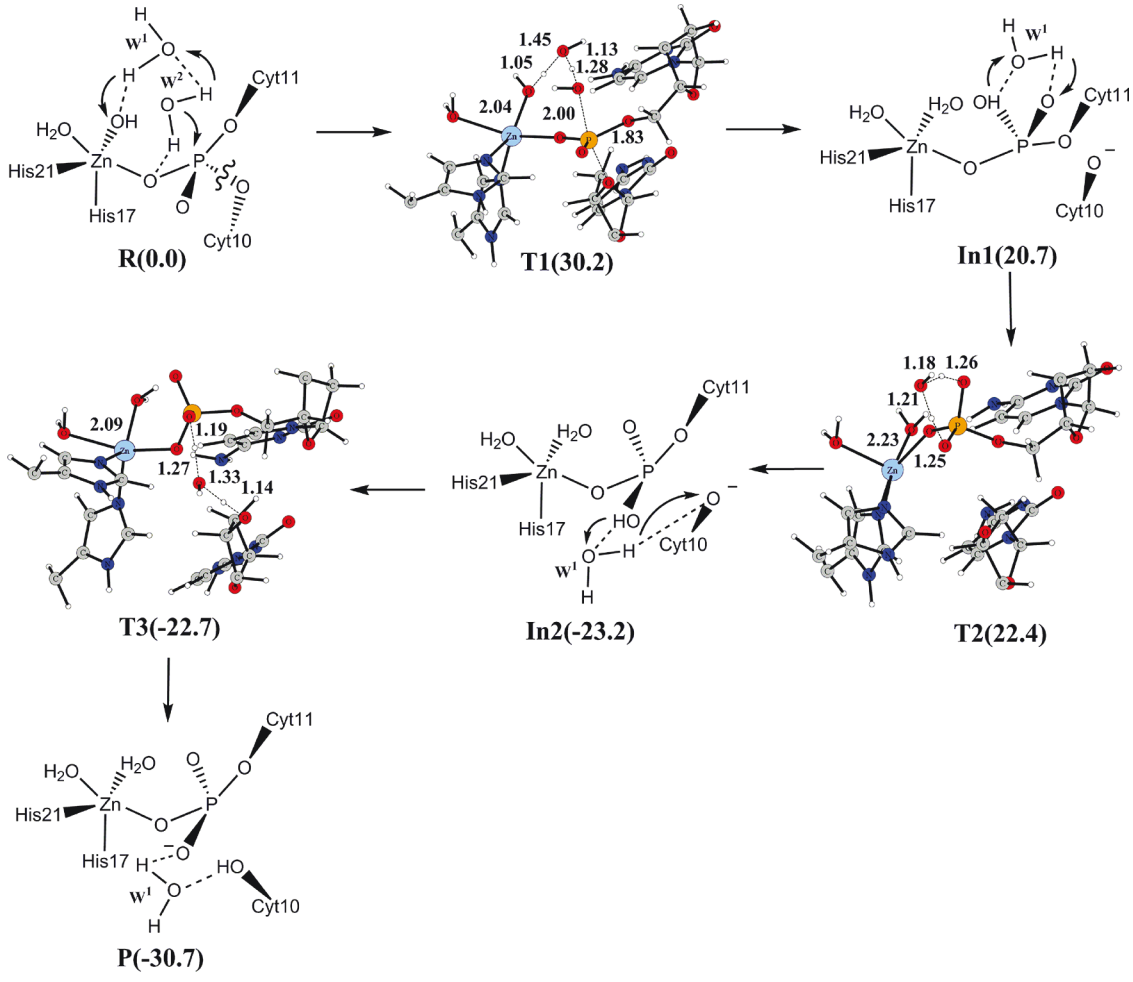

Figure 3. Proposed mechanism for the DNA hydrolysis by the ClavA−Zn complex.

phosphate group of DNA (Figure 3). The binding of a water molecule to the Zn(II) ion and the interactions with another water and phosphate groups significantly lower its pK_a value. This lowering of the pK_a of water to generate a hydroxyl nucleophile through metal coordination and hydrogen bonding is a common feature of metallohydrolases.[36,37] Additionally, two water molecules (W^1 and W^2) are also present at the active site. These water molecules form a hydrogen bond network between the Zn(II) bound OH group and the phosphate groups, including Cy10 and Cyt11 of DNA (Figure 2). Furthermore, due to the Lewis acidity of the Zn ion, the scissile P−O bond (1.53 Å) of DNA in **R** is elongated by 0.05 Å in comparison to the bond (1.48 Å) in its free form. In the first step, the Zn(II) bound OH functions as a base and abstracts a proton from W^2 through the bridging W^1 water, i.e., the $W^2 \rightarrow W^1 \rightarrow$ OH(Zn) pathway. This chain of proton transfer causes the formation of a nucleophile (−OH) close to the phosphate group, which simultaneously attacks the electrophilic phosphorus (P) atom and cleaves the scissile phosphoester [P−O(Cyt10)] bond (Figure 3). This concerted

https://dx.doi.org/10.1021/acsinfecdis.0c00051
ACS Infect. Dis. 2020, 6, 1250−1263

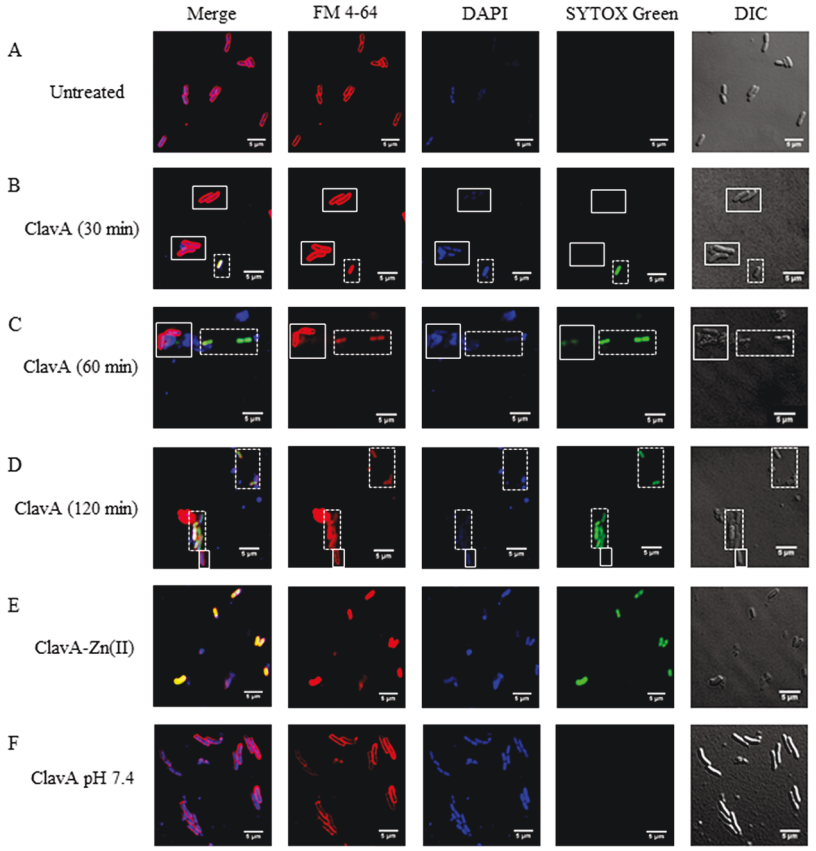

Figure 4. Micrographs of *E. coli* that have been (A) untreated or treated with (B) ClavA for 30 min, (C) ClavA for 60 min, (D) ClavA for 120 min, (E) ClavA–Zn(II) for 60 min, and (F) ClavA for 60 min at neutral pH. Scale bars are 5 μm. Solid white boxes indicate ClavA Type A_1, while dashed white boxes indicate Type A_2.

process occurs with a barrier of 30.2 kcal/mol, and the optimized transition state (**T1**) is shown in Figure 3. This is the rate-limiting step of the entire mechanism. The reason for this high barrier is the low acidity of W^2 in the major groove. The removal of W^1 in the model significantly increases the barrier for this process by 6.2 kcal/mol, i.e., 36.4 kcal/mol from the corresponding reactant. Additionally, a direct attack by the Zn(II) coordinated −OH nucleophile, without the assistance of both W^1 and W^2, takes place with a barrier further higher by 11.1 kcal/mol, i.e., 41.3 kcal/mol from the reactant. These results show that in this ligand environment the Zn(II) bound −OH is a weak nucleophile. Furthermore, the formation of the pentavalent phosphorane intermediate created by the direct Zn(II)−OH nucleophilic attack is endothermic by 45 kcal/mol. In the intermediate (**In1**), formed through **T1**, one of the DNA strands is broken to create a negatively charged cytosine ($Cyt10O^-$) fragment (Figure 3). Since this charged fragment is not a good leaving group, the formation of **In1** is endothermic by 20.7 kcal/mol from **R**. Due to the bulkiness of the $Cyt10O^-$ fragment, it cannot move and accept a proton from the −OH nucleophile that is now coordinated to the P atom. Therefore, the neutralization of this fragment requires two additional steps. In the next step, from **In1**, the proton from the nucleophile through W^1 is transferred to the nonesterified O atom. This step occurs with a small barrier of 1.7 kcal/mol from **In1**, and the optimized transition state (**T2**) is shown in Figure 3. The intermediate (**In2**) formed in this step is exothermic by 23.2 kcal/mol from the reactant **R**. In **In2**, the Cyt10 fragment is ideally located to abstract the O^1H proton. In the final step, this transfer takes place with an extremely low barrier of 0.5 kcal/mol from **In2** (Figure 3). The product (**P**) with the neutral form of the Cyt10 fragment is exothermic by 30.7 kcal/mol.

Kinetic Isotope Effects Support the Computationally Derived Mechanism. In order to validate the results of our computational calculations, we performed DNA cleavage experiments with ClavA–Zn(II) in H_2O and D_2O as solvents (Figure S4). The rate constants were calculated for each with $k_{H_2O} = 9.17 \times 10^{-5}$ s^{-1} and $k_{D_2O} = 3.67 \times 10^{-5}$ s^{-1}, resulting in an isotope effect of 2.5. This solvent isotope effect is consistent with the proposed mechanism in which one or more of the proton transfer steps are fully or partially rate limiting.

Phenotypic Analysis Reveals Multiple ClavA Mechanisms of Action. Despite the compelling evidence indicating that ClavA is capable of cleaving DNA in the presence of zinc ions, it cannot be ignored that almost all of the published research on the HDP indicates that it is membrane active.[10−13] We have shown previously that ClavA has antimicrobial activity in the absence of zinc ions, which would indicate that ClavA has at least two mechanisms of action depending on the environment of the peptide. In order to further explore the mechanisms employed by ClavA, we hypothesized that bacterial cytological profiling (BCP) will allow for the observation and differentiation of the ClavA mechanisms of action. BCP is based on the idea that antibiotics that act on the same pathway or target will likewise cause the same phenotypic changes in treated bacteria.[38] This technique has been

https://dx.doi.org/10.1021/acsinfecdis.0c00051
ACS Infect. Dis. 2020, 6, 1250−1263

Table 2. Summary of the ClavA Mechanisms of Action

Damage Type		General Features
Type A_1		Slightly longer than untreated *E. coli*, normal ring-shaped membrane
Type A_2		Diffuse membrane staining, blue and green stained DNA
Type N	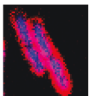	Longer than Type A_1, most cells have two nucleoids, normal membrane

previously applied to the study of the MoA for small molecule antibiotics and anticancer metal−ligand complexes.[39,40]

The study of the antimicrobial effect of any molecule via BCP begins with phenotypic analysis of the treated cells. The first step in this process is to collect and analyze micrographs of *E. coli* treated with ClavA. The morphology of the bacterial membranes was measured via staining with FM 4-64 (Figure 4, red), and its permeability was reported by SYTOX green (Figure 4, green), a cell impermeable DNA dye. The cell permeable DNA stain DAPI (Figure 4, blue) was also used to identify and measure nucleoid morphology and multiplicity. These images are analyzed for size and shape of the membrane and nucleoid as well as the relative intensity of the DNA dyes.

After treating *E. coli* with ClavA for 60 min at pH 5.5, we observed two distinct phenotypes (Figure 4C). The first phenotype, indicated by the solid white box, was longer than the untreated *E. coli* (Figure 4A) but maintained the same overall appearance with a ring of red for the membrane and blue DNA inside. Cells displaying the second phenotype, indicated by the dashed white box, maintained a similar overall size to the untreated cells but with a diffuse red signal throughout and with DNA stained both blue and green. We called these two phenotypes Type A_1 and Type A_2, respectively, due to the acidic pH at which they are observed. Approximately 60% of the cells show Type A_1 damage and the remaining 40%, Type A_2 after 60 min of treatment (ClavA damage types are summarized in Table 2). On the basis of these results, we conclude that, at low pH, ClavA is actually working via two different mechanisms of action.

We hypothesized that these two mechanisms of bacterial damage were based on exposure time to ClavA. To test this, we modified the treatment time from the original 60 min to 30 and 120 min, represented by Figure 4B,D, respectively. After 30 min of treatment, the predominant MoA for ClavA is Type A_1, with about 80% of cells falling into that category. The ratio flips at 120 min, with 75% of the cells exhibiting the Type A_2 phenotype. This would indicate that the initial interaction of ClavA with *E. coli* results in Type A_1 damage, with Type A_2 appearing after, and possibly as a result of, Type A_1.

Since ClavA is potentiated by Zn(II) at low pH, we next determined if and how the addition of Zn(II) affected the phenotype of the treated *E. coli*. As can be seen in Figure 4E, ClavA−Zn(II) treatment results exclusively in damage resembling Type A_2. The visual similarities between *E. coli* treated with ClavA−Zn(II) and Type A_2 damage point to the likelihood that these two mechanisms are the same and that the Type A_2 MoA results from scavenging Zn(II) ions from *E. coli* or the media.

Next, we determined if and how these mechanisms differ from the activity of ClavA at neutral pH since van Kan et al. postulated a different MoA under those conditions, namely, nonspecific pore formation.[13] Figure 4F shows cells treated with ClavA at pH 7.4. It can be observed that these cells are longer than either untreated or ClavA Type A_1 damaged *E. coli* and that most (∼88%) of these cells have two nucleoids (Figure 4F). The MoA that resulted in this visually distinct phenotype is referred to as ClavA Type N, due to the neutral pH at which this phenotype appears.

Identification of Mechanisms of Action through Principal Component Analysis. For a more quantitative approach to data analysis, we employed principal component analysis (PCA), which is a statistical treatment that reduces the dimensionality of a large data set, while minimizing the loss of variance. In this procedure, the set of measurements of possibly correlated variables are orthogonally transformed into values of uncorrelated variables, called principal components. The first principal component reflects the variable with the highest variance, followed by the second principal component with the second highest variance, and so on. Commonly, the values of the first, second, and third principal components are used for presenting the visual 2D and 3D plots. We have elected to use the 2D plot as the variance in the third dimension was minimal.

Figure 5 shows a PCA plot of the data pertaining to the various mechanisms of action for ClavA presented above. (Data collected for all treatments and used for PCA can be found in Tables S2 and S3.) It is clear from the plot that Type

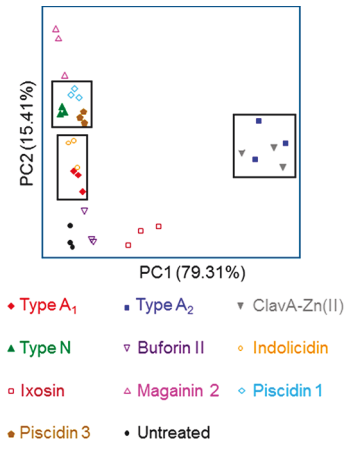

Figure 5. PCA plot of the ClavA treatments with model AMPs. The boxes indicate treatments that cluster together.

https://dx.doi.org/10.1021/acsinfecdis.0c00051
ACS Infect. Dis. 2020, 6, 1250−1263

A_1 and Type N are found in different regions of the plot, while Type A_2 and ClavA−Zn(II) cluster together. These results corroborate what was found through phenotypic analysis, namely, that Type A_1, Type A_2, and Type N mechanisms are all different and that the MoA corresponding to Type A_2 is the same as that of ClavA−Zn(II).

PCA can be more informative when used in conjunction with treatments of a known MoA. When these established treatments cluster with the treatment of interest, it indicates that their mechanisms of action likely share the same target molecule or pathway. For this study, we used six HDPs with well-defined mechanisms of action: (i) magainin 2, a membrane active HDP known to form toroidal pores in the membranes of both Gram-positive and Gram-negative bacteria;[41−43] (ii) buforin II, an HDP that binds to DNA after crossing the cellular membrane of bacteria without damaging it;[44−46] (iii) indolicidin, a nonlytic peptide with an internal target capable of creating pores in the inner and outer membranes of Gram-negative bacteria;[47,48] (iv) ixosin, an HDP that exerts its activity against the membrane through oxidative damage utilizing bound Cu(II), resulting in membrane perturbation;[49,50] and (v−vi) piscidin 1 and 3, which have been shown to bind both the membrane and DNA.[51] Piscidin 1 interacts more strongly with the membrane, while piscidin 3 interacts more strongly with DNA. Micrographs for each of the established HDPs can be found in Figure S5.

On the basis of the varied mechanisms of action presented above, it is no surprise that all of our model peptides localize in different parts of the PCA plot (Figure 5). ClavA Type A_1 clusters with indolicidin, indicating that Type A_1 damage is likely similar to that inflicted by indolicidin. ClavA Type N clusters with piscidin 1 and 3 but does not cluster with magainin 2. This indicates that ClavA at neutral pH interacts with the membrane in a manner similar to the two piscidins, and it does not form pores akin to magainin 2 as previously believed.[13] In contrast with both Type A_1 and Type N, Type A_2 does not cluster with any of the established peptides and instead only clusters with ClavA−Zn(II), which serves to emphasize the uniqueness of the MoA proposed for ClavA−Zn(II) and supports the observation that these mechanisms of action are the same from the phenotypic analysis.

Membrane Interaction Studies Reveal the Lack of Pore Formation in Model Membranes. While we have explored in detail the MoA of ClavA TypeA_2, it is also important to take a closer look at Type N and Type A_1. Considering both of these have been described previously by van Kan et al. as membrane based and each clusters with HDPs that have membrane activity as a part of their MoA, we decided to explore how ClavA interacts with the membrane at pH 7.4 and 5.5.[13] First, we performed circular dichroism (CD) spectroscopy in the presence of lipid vesicles in order to study the interaction of the peptide with the membrane, the results of which are summarized in Figure 6. (Full CD spectra can be found in Figure S6.) At pH 5.5, ClavA achieves over 90% α-helical content at a peptide to lipid ratio of 1:80, while at pH 7.4, only about 40% α-helix is observable. The K_d values for the peptide membrane interactions at pH 5.5 and 7.4 are 330 ± 20 and 390 ± 30 μM, respectively, which indicate that while the interactions at low and neutral pH are clearly different, as shown by the difference in helical content, they are roughly the same overall strength.

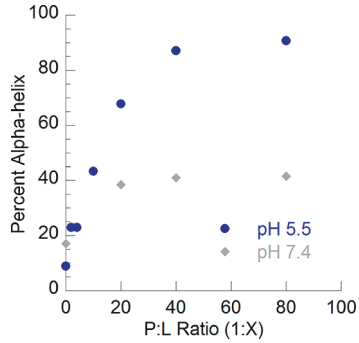

Figure 6. α-Helical content vs peptide to lipid ratio as determined by CD spectroscopy. *X*-axis values are the lipid portion of the peptide to lipid ratio.

Many membrane active HDPs have been reported to form pores, especially magainin 2, while others, such as piscidin 1 and 3, can insert into the membrane and kill bacteria without the formation of transmembrane pores. With this in mind, we next sought to determine if nonmetalated ClavA behaves more like the former or the latter. The techniques employed in this determination were X-ray diffraction (XRD) and combined surface plasmon resonance and electrical impedance spectroscopy (SPR/EIS). XRD was employed in order to look for the presence of membrane thinning, usually associated with the formation of transmembrane pores. SPR/EIS performed on tethered bilayer membranes allows for simultaneous detection of the interaction of ClavA with the membranes (SPR) as well as pore formation through decreased resistivity (EIS). The results of XRD experiments (Figure S7A) indicate that, at pH 7.4, ClavA appears to remain on the surface of the membrane, resulting in membrane thickening, which is in direct contrast to the membrane thinning observed for magainin 2.[52] Additionally, SPR/EIS indicates that the ClavA interaction with the membrane does not result in the formation of pores (Figure S7B). In fact, ClavA appears to increase the resistivity of the membrane, the opposite effect of what would occur during pore formation. These results together indicate that, while ClavA may be interacting with the membrane, it is doing so in a way that is fundamentally different from magainin 2. Further study of the effect of the ClavA interaction with bacterial membranes is necessary to fully understand what is occurring in the Type N and Type A_1 mechanisms.

■ DISCUSSION

In this study, we were able to more definitively prove a hypothesis we presented in our previously published work;[9] namely, not only is the antimicrobial activity of the HDP ClavA potentiated by the presence of zinc ions, but also ClavA−Zn(II) is capable of functioning as a metallonuclease within live bacteria. We were also able to propose a probable mechanism for the cleavage of DNA through the application of the QM/MM method. This mechanism is particularly novel, as most metallonucleases cleave DNA via activated water molecules in the primary coordination sphere, whereas ClavA−Zn(II) utilizes a secondary coordination sphere water molecule to cleave the phosphoester bond in the DNA backbone.

In addition to all of the mechanistic work on ClavA, we were also able to expand the scope of the Zn(II) based potentiation of ClavA to encompass not only *E. coli* but also all of the Gram-negative ESKAPE pathogens, including some multidrug-

https://dx.doi.org/10.1021/acsinfecdis.0c00051
ACS Infect. Dis. 2020, 6, 1250−1263

resistant clinical isolates. These results seem to imply that ClavA−Zn(II) will show a similar potentiation against all Gram-negative pathogens. This finding is of particular importance as Gram-negative bacteria are particularly difficult to treat with conventional methods due to their double membrane structure.[21] Gram-negative bacteria have a significantly lower success rate than Gram-positive bacteria when it comes to drug screening tests, with *P. aeruginosa* reporting up to 1000-fold fewer successes than Gram-positive pathogens.[53] The successful application of ClavA−Zn(II) to the treatment of these difficult pathogens could help to encourage the development of peptidic antibiotics for the treatment of Gram-negative infections as well as the development of new strategies for bypassing the particularly resilient Gram-negative membrane.

Many transition metals, when presented in sufficient quantities, have proven to be toxic to bacteria, and zinc is no exception. We have shown that the MIC values for Zn(II) against the bacteria used in this study are all in the low millimolar range, while in the MIC experiments for ClavA−Zn(II), the highest concentration of Zn(II) used is 512 μM. When the fractional inhibitory concentration (FIC) is calculated, it is clear that the interaction of ClavA with Zn(II) ions is synergistic, with bacterial growth inhibition occurring at much lower concentrations than for each alone.

We were also able to bridge the gap between our results, which show that ClavA can act on DNA, which results in growth inhibition, and the results first proposed by van Kan et al. that provide evidence for ClavA as a membrane active peptide.[13] We accomplished this through the utilization of BCP. As a means of studying mechanisms of action, BCP has been utilized with small molecule antibiotics and anticancer organometallic compounds, but never before has BCP been applied to the study of HDPs.[38,40] Through the application of BCP, we were able to determine that ClavA has at least three different mechanisms of action, which are dependent on pH and zinc concentration.

ClavA is not the first instance of a peptide for which the literature appears to conflict regarding the MoA, especially when the apparent disagreement is between membrane based and internal mechanisms of action. For example, indolicidin was first believed to create membrane pores for its antimicrobial activity.[54] It was later discovered that indolicidin can bind to DNA, interfering with replication, transcription, and translation.[47] It is likely that with varied treatment conditions, including incubation time and peptide concentration, BCP would result in different phenotypes for indolicidin treated cells. Another HDP for which the literature is inconsistent is tachyplesin, which has been shown to target LPS, membrane phospholipids, and the minor groove of DNA.[55−58] Piscidin 3 has been shown to be membranolytic, as are many members of the piscidin family, though the MIC has been shown to be largely controlled by a DNA based MoA.[59−61] The fungal defensin, plectasin, has also been identified to act on two distinct targets; though in contrast to the other examples presented above that show the membrane and DNA as the primary targets, plectasin has been shown to bind Lipid II, inhibiting cell wall biosynthesis and membrane embedded potassium ion channels.[62−64] In each of these cases, the application of BCP could streamline the process of determining the MoA, though it is necessary to have a set of peptides with well-defined and agreed upon mechanisms of action, such as buforin II and magainin 2, before this method can be applied on a larger scale.

Together, the data presented in this study and the previous work on ClavA[9,13] allow us to propose the following as the most complete MoA for ClavA to date (Figure 7). At neutral pH, ClavA exerts its activity by causing nonspecific membrane damage, likely resulting in the loss of the proton motive force and the leakage of cellular contents (Type N, Figure 7A). This activity is supported by the clustering of Type N with the piscidins in the PCA plot (Figure 5) as well as work performed by van Kan et al., which shows that, at neutral pH, ClavA can dissipate the transmembrane potential and can cause leakage of calcein from model membranes.[13] On the basis of the elongated appearance of the cells treated at pH 7.4 (Figure 4F), this activity appears to inhibit the ability of *E. coli* to properly divide.

When the pH is lowered to 5.5, as typically happens in phagosomes, the mechanism changes to involve binding to membrane embedded ion channels, as presented by Juliano et al. and van Kan et al. (Figure 7B).[9,13] Additionally, we have shown via CD that there is a strong membrane interaction at pH 5.5 (Figure S6A), which could allow the translocation of ClavA into the cytoplasm. Once there, ClavA binds to DNA

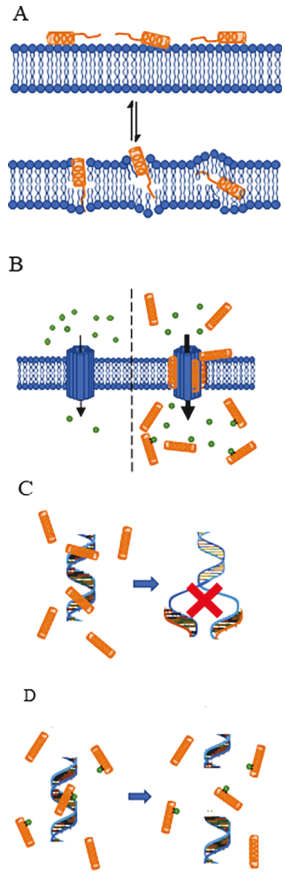

Figure 7. MoA of ClavA (A) at neutral pH (Type N) involves membrane disruption as previously proposed.[6] (B, C) Type A_1 at pH 5.5 starts with the proposed binding of ClavA to the ionophores, distorting their gating[6] followed by indolicidin like DNA synthesis inhibition, and (D) Type A_2 at pH 5.5 in which ClavA−Zn(II) cleaves DNA as previously shown.[2] Orange helices represent ClavA; green circles represent Zn(II) ions.

https://dx.doi.org/10.1021/acsinfecdis.0c00051
ACS Infect. Dis. 2020, 6, 1250−1263

and inhibits DNA synthesis in a similar manner to indolicidin, which is supported by Figure 5 (Type A_1, Figure 7C).

The interaction of ClavA with currently unidentified transmembrane ion channels has some effect on their gating, allowing the free exchange of ions between the cytoplasm and the extracellular space. It is this change to ion permeability that likely allows for an increase in the intracellular Zn(II) concentration in bacteria (Figure 7B). ClavA, either free floating or DNA bound, can bind to some of the newly increased concentration of Zn(II) ions, allowing for subsequent DNA hydrolysis (Type A_2, Figure 7D). Clavanins were isolated from phagocytic cells of *S. clava* and postulated to be delivered into their phagosomes when required.[65,66] Although there are no reports on zinc ion trafficking inside *S. clava* phagocytic cells, high micromolar concentrations of free zinc ions have been shown to accumulate inside phagosomes of macrophages in response to certain bacterial pathogens or stimuli.[67,68] It is likely that the phagocytic cells in which the Clavanins are found to behave in a similar fashion to their murine and human counterparts. ClavA has also been found in cytoplasmic granules, which are commonly secreted at the site of infection.[66] In conditions outside of the Zn(II) enriched phagosome, ClavA would need to get Zn(II) from the bacteria themselves; however, the free pool of zinc ions within a bacterium is low, with most of the zinc bound within bacterial enzymes and virulence factors.[69,70] One possible explanation for why ClavA exhibits these multiple mechanisms of action is that, in order to have free Zn(II) available to bind, ClavA needs to first kill some of the bacteria via a different MoA, thereby increasing the local concentration of labile Zn(II) ions.

Type A_1 on its own would likely be only bacteriostatic, though this cannot be observed because ClavA will eventually scavenge Zn(II) ions from the bacterium or surrounding media, resulting in the Type A_2 mechanism. This is supported by the previously reported time kill kinetics data in which ClavA caused culture sterilization in 4 h, while ClavA−Zn(II) accomplished the same feat in half the time.[9] The potentiated activity that is observed when Zn(II) is added to the culture medium comes from the increased availability of those zinc ions. The proposed mechanisms also explain the 16-fold decrease in MIC as normally ClavA needs to get inside and scavenge Zn(II) from the bacterium.

As with all mechanistic studies on HDPs, it is important to note here that one MoA cannot fully characterize the behavior of a population of HDPs. This has been shown recently in a study utilizing bacterial spheroplasts to study the localization of buforin II and magainin 2.[71] In this work, it is highly possible that, in our low pH experiments, some small percentage of the ClavA population may never transition from Type A_1 to Type A_2. It may mean that the cells treated with that subset survive, or they may be killed through a yet undiscovered mechanism.

CONCLUSIONS

In conclusion, we demonstrate through *in cellulae*, *in silico*, and *in vitro* assays that the tunicate HDP, Clavanin A, uses Zn(II) ions to achieve DNA damage. QM/MM calculations predicted the nucleophilic attack of a hydroxyl group to an electrophilic phosphorus to cleave the scissile phosphoester bond with an activation energy of 30.2 kcal/mol; a prediction that is bolstered by the observed normal kinetic isotope effect. Combined phenotypic analysis, CD spectroscopy, and SPR/EIS show that Clavanin A is a "dirty" drug, using three mechanisms of action to inhibit the growth of Gram-negative bacteria. The identification that ClavA−Zn(II) showed improved activity against multidrug-resistant clinical isolates provides further evidence that metallopeptides constitute a promising antimicrobial family, and additional studies are warranted to fully elucidate their mechanisms of action and potential therapeutic applications. The evidence of synergy between ClavA and Zn(II) and the other results presented above inform on the literature for metallopeptides and, in addition, show the utility of studying known HDPs in the presence of biologically relevant metal ions, including Cu(II), Fe(II), and Zn(II).

MATERIALS AND METHODS

Bacterial Culture Conditions. Bacteria treated under low pH conditions were grown in LB media containing 50 mM MES buffer at pH 5.5. For the neutral pH experiments, bacteria were grown and treated in standard MHB media at pH 7.4. Cells were incubated at 37 °C and 234 rpm to mid log phase (OD_{600}= 0.4−0.6).

Minimum Inhibitory Concentration Determination. Minimum inhibitory concentrations (MICs) for ClavA and ClavA−Zn(II) were determined via the broth microdilution method, which has been previously described.[72] Briefly, bacteria were grown to mid log phase (OD_{600}= 0.4−0.6), diluted to a final concentration of 1×10^6 cfu/mL, and treated with serially diluted peptide for 18 h. All of the growth media used contained 50 mM MES buffer at pH 5.5. MIC was determined as the concentration of peptide at which no growth could be visually observed. The data presented represent the mode of three trials. For all experiments containing ClavA−Zn(II), the peptides were incubated with $ZnCl_2$ for 30 min at room temperature at 2× the maximum concentration used, with the maximum zinc concentration of any of these assays being 512 μM.

When the MIC values for Zn(II) were determined, a similar process was utilized. Diluted bacteria were treated with $ZnCl_2$, and MICs corresponded to the lowest concentration at which no growth could be observed visually. Values were measured at pH 5.5 and 7.4 and were found to be identical. Results represent the mode of three trials.

TUNEL Assay. The TUNEL assay has been described previously.[73] Briefly, an overnight culture of *E. coli* was washed in PBS. The cells were then treated with MIC concentrations of ClavA and ClavA−Zn(II), with aliquots removed at 1, 2, and 4 h. A negative control was performed with PBS and a positive control, with 0.75% H_2O_2. After incubation, cells were fixed and dyed; then, propidium iodide and fluorescein labeled cells were measured via flow cytometry. Data presented represent the average of three trials, and the error bars are standard error from the mean.

Computational Details. *Molecular Dynamics (MD) Simulations.* The structure of ClavA was obtained from the protein data bank (PDB ID: 6C41).[74] The initial ClavA−Zn(II) structure in which His17 and His21 were coordinated to the Zn ion was built and energy minimized using the YASARA software.[75] The CAAGACGGCCCCGGCCC nucleotide sequence[76] of *E. coli* TD172 DNA was built using the Avogadro software.[77] The HDOCK Web server was used to explore the binding poses of the ClavA−Zn(II) complex to DNA.[78] In all the docked structures, ClavA−Zn(II) was located in the major groove of DNA. Two different ClavA−Zn binding poses were used as the starting structures for molecular dynamics (MD) simulations: i.e., (1) ClavA−Zn(II) is bound

https://dx.doi.org/10.1021/acsinfecdis.0c00051
ACS Infect. Dis. 2020, 6, 1250−1263

in a perpendicular manner inside the major groove of DNA, and (2) ClavA−Zn(II) is bound parallel to the major groove of DNA (Figure S8). All 200 ns all-atom MD simulations in aqueous solution were performed using the GROMACS-4.5.6[79] program utilizing the CHARMM36[80] force field. This force field was reported to reproduce the key structural features of ClavA and ClavA−Zn(II) in our previous work.[81] The ClavA−Zn−DNA complex was placed in the cubic box of 10 × 10 × 10 nm dimension. The shortest distance from the edge of the box to the surface of the complex was 1.0 nm. The Particle Mesh Ewald method[82] was used to compute the electrostatic interactions, and for both Coulombic and van der Waals interactions, a 1.2 nm cutoff distance was maintained. TIP3P[83] water was used as a solvent, and Na^+ and Cl^- were added to neutralize and to maintain the physiological ion concentration (154 mM) of the system. The starting structures for MD simulations were energy minimized for 3000 steps using the steepest descent method. The simulations were performed using a constant number of particles (N), pressure (P), and temperature (T), i.e., NPT ensemble. SETTLE[84] algorithm was used to constrain the bond length and angle of the water molecules, and LINCS[85] algorithm was employed to constrain the remaining bond lengths. The trajectories were computed for each model with a time step of 2 fs. Cluster analysis was utilized to obtain the most representative ClavA−Zn(II)−DNA structure from the MD simulations. The ClavA−Zn(II) and DNA binding energies were calculated by utilizing the Molecular Mechanics Poisson−Boltzmann Surface Area (MM-PBSA) method.[86] A comparison of the binding energies shows that the structure in which ClavA was bound in a perpendicular fashion inside the major groove of DNA is 37.0 kcal/mol lower in energy than the second structure (Figure S8).

QM/MM Calculations. All hybrid two-layer QM/M (ONIOM) calculations were performed using the Gaussian 09 (ONIOM) software package.[87] ONIOM utilizes a subtractive method in which the MM energy [E_{MM} (model)] of the QM (model) part is subtracted from the sum of the QM energy of the model [E_{QM} (model)] and MM energy [E_{MM} (real)] of the whole (real) system, i.e., E_{ONIOM} (QM/MM) = E_{QM} (model) + E_{MM} (real) − E_{MM} (model). This subtraction method corrects the artifacts introduced by the link atom.[28] The ONIOM optimization procedure uses macro/micro-iterations,[29] and the electrostatic interactions between the QM and the MM part were treated by mechanical embedding (ME). The QM region was composed of a Zn(II) ion, His17, His21, two cytosine nucleotides, a hydroxyl ion, and one to three water molecules (depending on the reaction mechanism) as shown in Figure 2. The remaining part of the system was included in the MM layer. The ClavA−Zn−DNA complex was surrounded with explicit water molecules (2139 water molecules; MM layer) to stabilize the highly negative charge of DNA. The QM layer was optimized without any geometric constraints using the hybrid B3LYP[88] exchange-correlation functional. The Lanl2dz basis set (for the Zn atom) with the corresponding Hay-Wadt effective core potential (ECP)[89] and the 6-31G(d) basis set (for the remaining atoms in the QM layer) were used. The MM layer was modeled using the AMBER force field.[90,91] The energies of the optimized structures were further improved by performing single-point calculations using the large basis sets, e.g., Lanl2tz for Zn and triple-ζ 6-311+G(d,p) for other atoms. Hessians were calculated at the same level of theory as the optimizations to confirm the nature of the stationary points along the reaction coordinate. The transition states were confirmed to have only one imaginary frequency corresponding to the reaction coordinates. Zero-point vibrational, thermal, and entropy corrections were added to the final energies (at 298.15 K and 1 atm). The helical wheel projection of ClavA was obtained from NetWheel online Web server.[92] VMD,[93] YASARA,[75] ChemDraw, and Chimera[94] programs were used for the visualization of the MD trajectories and preparation of the figures used in this study.

DNA Cleavage. DNA cleavage experiments were performed as previously described.[9] Briefly, 10 μM base pair pUC19 was incubated with 1 μM ClavA−Zn(II) for the indicated times in MES buffer at pH 5.5. The reaction was stopped using 3× loading dye containing 1 mM EDTA prior to loading on the 1% agarose gel containing ethidium bromide, and the gel was run at 100 V for 90 min. Gels were imaged using a Bio-Rad GelDoc XR+ Imager and quantified using Image Lab 5.0 software. D_2O samples were prepared from samples dissolved in H_2O by lyophilization and dissolution in D_2O. This was repeated 3 times to ensure solvent exchange.

The kinetic isotope effect was determined by plotting the concentration of supercoiled pUC19 vs time in order to obtain rate constants for D_2O and H_2O. The kinetic isotope effect was then calculated by dividing k_{H_2O} by k_{D_2O}.

Confocal Fluorescence Microscopy. *E. coli* cultures were inoculated in culture media described above and grown to an OD_{600} of about 0.5 and treated with equal volumes of host defense peptides (HDPs) at a final concentration of each peptide's MIC value. These were incubated for 1 h on a shaking incubator at 37 °C, followed by staining with 1 μg/mL FM 4-64, 2 μg/mL DAPI, and 0.5 μM SYTOX Green for 30 min. FM 4-64 selectively stains bacterial membranes while DAPI and SYTOX Green both stain DNA and are cell permeable and impermeable, respectively.

These changes from the protocol by Nonejuie et al.[38] were required because many HDPs have been shown to completely sterilize cultures at time scales between 1 and 2 h. Additionally, with several of the HDPs tested, few bacteria remained when treated with concentrations of 5× MIC of the peptides.

After staining, the cultures were concentrated via centrifugation at 14 000 rpm for 90 s and resuspended in 1/10 their original volume. Three microliters of the culture was then spotted onto 1.5% agarose pads containing 20% LB medium; the sample was then prepared using 65 μL gene frame seals on microscope slides. The cells were then imaged using a Nikon A1R spectral confocal microscope with a 60× oil immersion lens.

Bacterial Cytological Profiling. Bacterial cytological profiling (BCP) was performed using a procedure adapted from Nonejuie et al.[38] All cellular measurements were performed using ImageJ software, utilizing the freehand selection tool to trace either the membrane or nucleoid. Each was then measured for area, perimeter, and circularity. Length and width were measured separately using the straight-line selection tool. Average DAPI and SYTOX Green intensities were measured using the outline of the membrane and subtracted from the background intensity. The intensities were then normalized against the intensities from untreated cells measured on the same day with the same microscope and camera settings. In every case, measurements were made on at least 50 cells, and every cell was measured in each image used, excluding any cells that we only partially captured.

https://dx.doi.org/10.1021/acsinfecdis.0c00051
ACS Infect. Dis. 2020, 6, 1250−1263

Principal Component Analysis. For each antimicrobial treatment, the cell morphology parameters were obtained from at least three independent experiments. For each parameter, the average measurement was also calculated and included in the data set. The parameters were reduced into three orthogonal variables using principal component analysis (PCA) from our in-house Python scripts. For each treatment, three cells were selected as representative cells by determining three transformed measurements with the shortest Euclidean distance from the transformed average measurement. The cell morphology parameters of the representative cells were used for PCA of various groups of treatments. Clustering was performed using the Euclidean distance method from our in-house Python scripts, where centroids having a distance of 2.4 units or lower are in the same cluster.

Circular Dichroism. CD spectroscopy was used to monitor the titration of ClavA with 3:1 1-palmitoyl-2-oleoyl-glycero-3-phosphocholine (POPC)/POPG large unilamellar vesicles (LUVs) in phosphate buffer at acidic (pH 5.5) and neutral (pH 7.4) pHs. LUVs were prepared at both pHs as follows. Lipid films were made by mixing in a round-bottom flask appropriate volumes of POPC and POPG lipids solvated in chloroform. The chloroform was then evaporated under a flow of nitrogen gas prior to lyophilization overnight. The dried lipid films were hydrated with buffer (buffer concentrations of 2.5 mM, pH 5.5, or 5 mM, pH 7.4), producing 5 mM lipid suspensions. After several freeze−thaw cycles (incubation in a 40 °C oven, freezing in an ice bath), the suspensions were extruded using an Avanti Polar Lipids Mini Extruder (Avanti Polar Lipids, Alabaster, AL), resulting in vesicles with a diameter of 200 nm. The LUV suspensions were then diluted to 2 mM, and the vesicles were added to aqueous ClavA (321.00 μM) and buffer to obtain samples with seven P/L ratios between 1:0 and 1:80, each with a fixed peptide concentration of 20 μM. CD spectra were acquired by averaging three scans collected at 293 K on a J-1500 spectrometer (Jasco Analytical Instruments, Easton, MD) over a wavelength range of 190−260 nm using a scan speed of 100 nm/min and a 1 nm bandwidth. Spectra for buffer and phospholipid blanks without peptide were obtained at each P/L ratio and subtracted from the ClavA sample spectra to account for the background signal produced by the LUVs. Samples were made in triplicate (pH 5.5) or duplicate (pH 7.4) using the same batch of LUVs. The molar ellipticity obtained at 222 nm was converted into helicity, assuming an ellipticity of −32 000 deg·cm^2/dmol for a perfect helix and −2000 deg·cm^2/dmol for the fully disordered peptide.[95,96] Helicity was plotted in the form of a binding isotherm and fitted by a nonlinear least-squares minimization in Microsoft Excel 2016 using the Solver Add-in. Fit parameters included the binding constant, K_d, and the helical content of peptides in the free and bound state. A binding stoichiometry of 1:1 between peptides and lipids was used.

X-ray Diffraction Spectroscopy. Clavanin A was incubated with preformed 1-palmitoyl-2-oleoyl-glycero-3-phosphocholine (POPC; Avanti Polar Lipids) lipid vesicles at a peptide to lipid molar ratio of 1:25. The solution was fused onto glass coverslips, and bulk water was allowed to evaporate slowly overnight at room temperature, producing aligned lipid multilayers with incorporated peptide. Before diffraction experiments, the samples were annealed at 98% relative humidity and 30 °C for at least 12 h. X-ray diffraction measurements were performed on a 3KW Rigaku Smartlab diffractometer located at the Institute for Bioscience and Biotechnology Research (IBBR), Rockville, MD, as described previously.[97]

Surface Plasmon Resonance/Electrical Impedance Spectroscopy. Tethered lipid bilayer membranes (tBLMs) were prepared as described previously using POPC lipid.[98,99] The freshly prepared tBLM was stabilized in either TRIS buffer (20 mM TRIS, 50 mM NaCl, pH = 7.5) or MES buffer (50 mM MES, 50 mM NaCl, pH = 5.5) for SPR/EIS measurements at various pHs. Clavanin A was injected on top of the preformed tBLM in the corresponding buffer at a concentration of 3 μM and allowed to incubate with the bilayer for 10 min, followed by a buffer rinse. SPR/EIS spectra were collected simultaneously, as a function of time, as described previously.[97]

■ ASSOCIATED CONTENT

Supporting Information

The Supporting Information is available free of charge at https://pubs.acs.org/doi/10.1021/acsinfecdis.0c00051.

ClavA Zn(II) antimicrobial synergy; DNA gels; electrostatic surface potential and helical wheel projection of ClavA; root-mean-square-fluctuations (RMSFs) in the ClavA−Zn(II) complex; average morphology measurements; representative micrographs; circular dichroism spectra; X-ray diffraction, surface plasmon resonance, and electrical impedance spectroscopy; two MD equilibrated conformations (PDF)

■ AUTHOR INFORMATION

Corresponding Authors

Alfredo M. Angeles-Boza − *Department of Chemistry and Institute of Materials Science, University of Connecticut, Storrs, Connecticut 06269, United States;* orcid.org/0000-0002-5560-4405; Email: alfredo.angeles-boza@uconn.edu

Rajeev Prabhakar − *Department of Chemistry, University of Miami, Coral Gables, Florida 33146, United States;* orcid.org/0000-0003-1137-1272; Email: rpr@miami.edu

Authors

Samuel A. Juliano − *Department of Chemistry, University of Connecticut, Storrs, Connecticut 06269, United States*

Leonardo F. Serafim − *Department of Chemistry, University of Miami, Coral Gables, Florida 33146, United States*

Searle S. Duay − *Department of Chemistry, University of Connecticut, Storrs, Connecticut 06269, United States;* orcid.org/0000-0002-0382-1053

Maria Heredia Chavez − *Department of Chemistry, University of Connecticut, Storrs, Connecticut 06269, United States*

Gaurav Sharma − *Department of Chemistry, University of Miami, Coral Gables, Florida 33146, United States*

Mary Rooney − *Department of Applied Science, William and Mary, Williamsburg, Virginia 23187-8795, United States*

Fatih Comert − *Institute for Bioscience and Biotechnology Research, University of Maryland, Rockville, Maryland 20850, United States*

Scott Pierce − *Department of Chemistry, University of Connecticut, Storrs, Connecticut 06269, United States*

Andrei Radulescu − *Department of Chemistry, University of Connecticut, Storrs, Connecticut 06269, United States*

Myriam L. Cotten − *Department of Applied Science, William and Mary, Williamsburg, Virginia 23187-8795, United States;* orcid.org/0000-0002-6732-1736

https://dx.doi.org/10.1021/acsinfecdis.0c00051
ACS Infect. Dis. 2020, 6, 1250−1263

Mihaela Mihailescu − *Institute for Bioscience and Biotechnology Research, University of Maryland, Rockville, Maryland 20850, United States*

Eric R. May − *Department of Molecular and Cell Biology, University of Connecticut, Storrs, Connecticut 06269, United States;* orcid.org/0000-0001-8826-1990

Alexander I. Greenwood − *Department of Applied Science, William and Mary, Williamsburg, Virginia 23187-8795, United States*

Complete contact information is available at: https://pubs.acs.org/10.1021/acsinfecdis.0c00051

Notes

The authors declare no competing financial interest.

■ ACKNOWLEDGMENTS

The authors would like to thank the Venkietanarayanan Lab for donating *A. baumannii* Naval-17 and the CDC & FDA AR Isolate Bank for the donation of the multidrug-resistant clinical isolates.[23] We thank Dr. Vitalii Silin (IBBR) for help with SPR/EIS. This work was supported by the grants from the National Science Foundation (Grant MCB1715494 to A.M.A.-B. and Grant Number CHE1664926 to R.P.) and the National Institutes of Health (Grant R35GM119762 to E.R.M.).

■ REFERENCES

(1) OECD (2018) *Stemming the Superbug Tide,* DOI: 10.1787/9789264307599-en.

(2) Klevens, R. M., Edwards, J. R., Richards, C. L., Jr, Horan, T. C., Gaynes, R. P., Pollock, D. A., and Cardo, D. M. (2007) Estimating health care-associated infections and deaths in U.S. hospitals, 2002. *Public Health Rep. 122* (2), 160−166.

(3) Rice, L. B. (2008) Federal Funding for the Study of Antimicrobial Resistance in Nosocomial Pathogens: No ESKAPE. *J. Infect. Dis. 197* (8), 1079−1081.

(4) Santajit, S., and Indrawattana, N. (2016) Mechanisms of Antimicrobial Resistance in ESKAPE Pathogens. *BioMed Res. Int. 2016*, 2475067.

(5) Livermore, D. M. (2004) The need for new antibiotics. *Clin. Microbiol. Infect. 10* (Suppl 4), 1−9.

(6) Munoz-Price, L. S., Poirel, L., Bonomo, R. A., Schwaber, M. J., Daikos, G. L., Cormican, M., Cornaglia, G., Garau, J., Gniadkowski, M., Hayden, M. K., Kumarasamy, K., Livermore, D. M., Maya, J. J., Nordmann, P., Patel, J. B., Paterson, D. L., Pitout, J., Villegas, M. V., Wang, H., Woodford, N., and Quinn, J. P. (2013) Clinical epidemiology of the global expansion of Klebsiella pneumoniae carbapenemases. *Lancet Infect. Dis. 13* (9), 785−96.

(7) Silva, O. N., Fensterseifer, I. C., Rodrigues, E. A., Holanda, H. H., Novaes, N. R., Cunha, J. P., Rezende, T. M., Magalhaes, K. G., Moreno, S. E., Jeronimo, M. S., Bocca, A. L., and Franco, O. L. (2015) Clavanin A improves outcome of complications from different bacterial infections. *Antimicrob. Agents Chemother. 59* (3), 1620−1626.

(8) Silva, O. N., Alves, E. S. F., de la Fuente-Núñez, C., Ribeiro, S. M., Mandal, S. M., Gaspar, D., Veiga, A. S., Castanho, M. A. R. B., Andrade, C. A. S., Nascimento, J. M., Fensterseifer, I. C. M., Porto, W. F., Correa, J. R., Hancock, R. E. W., Korpole, S., Oliveira, A. L., Liao, L. M., and Franco, O. L. (2016) Structural Studies of a Lipid-Binding Peptide from Tunicate Hemocytes with Anti-Biofilm Activity. *Sci. Rep. 6*, 27128.

(9) Juliano, S. A., Pierce, S., deMayo, J. A., Balunas, M. J., and Angeles-Boza, A. M. (2017) Exploration of the Innate Immune System of Styela clava: Zn2+ Binding Enhances the Antimicrobial Activity of the Tunicate Peptide Clavanin A. *Biochemistry 56* (10), 1403−1414.

(10) Lee, I. H., Cho, Y., and Lehrer, R. I. (1997) Effects of pH and salinity on the antimicrobial properties of clavanins. *Infect. Immun. 65* (7), 2898−903.

(11) van Kan, E. J., van der Bent, A., Demel, R. A., and de Kruijff, B. (2001) Membrane activity of the peptide antibiotic clavanin and the importance of its glycine residues. *Biochemistry 40* (21), 6398−405.

(12) Silva, O. N., Alves, E. S., de la Fuente-Nunez, C., Ribeiro, S. M., Mandal, S. M., Gaspar, D., Veiga, A. S., Castanho, M. A., Andrade, C. A., Nascimento, J. M., Fensterseifer, I. C., Porto, W. F., Correa, J. R., Hancock, R. E., Korpole, S., Oliveira, A. L., Liao, L. M., and Franco, O. L. (2016) Structural Studies of a Lipid-Binding Peptide from Tunicate Hemocytes with Anti-Biofilm Activity. *Sci. Rep. 6*, 27128.

(13) van Kan, E. J., Demel, R. A., Breukink, E., van der Bent, A., and de Kruijff, B. (2002) Clavanin permeabilizes target membranes via two distinctly different pH-dependent mechanisms. *Biochemistry 41* (24), 7529−39.

(14) Gammoh, N. Z., and Rink, L. (2017) Zinc in Infection and Inflammation. *Nutrients 9* (6), E624.

(15) Vallee, B. L., and Falchuk, K. H. (1993) The biochemical basis of zinc physiology. *Physiol. Rev. 73* (1), 79−118.

(16) Richardson, C. E. R., Cunden, L. S., Butty, V. L., Nolan, E. M., Lippard, S. J., and Shoulders, M. D. (2018) A Method for Selective Depletion of Zn(II) Ions from Complex Biological Media and Evaluation of Cellular Consequences of Zn(II) Deficiency. *J. Am. Chem. Soc. 140* (7), 2413−2416.

(17) Sigel, A., Sigel, H., and Sigel, R. K. (2013) *Interrelations between essential metal ions and human diseases,* Springer.

(18) Prasad, A. S. (2008) Zinc in Human Health: Effect of Zinc on Immune Cells. *Mol. Med. 14* (5), 353−357.

(19) McDevitt, C. A., Ogunniyi, A. D., Valkov, E., Lawrence, M. C., Kobe, B., McEwan, A. G., and Paton, J. C. (2011) A Molecular Mechanism for Bacterial Susceptibility to Zinc. *PLoS Pathog. 7* (11), No. e1002357.

(20) (a) Wagner, D., Maser, J., Lai, B., Cai, Z., Barry, C. E., Höner zu Bentrup, K., Russell, D. G., and Bermudez, L. E. (2005) Elemental Analysis of Mycobacterium avium-, Mycobacterium tuberculosis-, and Mycobacterium smegmatis-Containing Phagosomes Indicates Pathogen-Induced Microenvironments within the Host Cell's Endosomal System. *J. Immunol. 174* (3), 1491. (b) Alexander, J. L., Thompson, Z., and Cowan, J. A. (2018) Antimicrobial Metallopeptides. *ACS Chem. Biol. 13* (4), 844−853.

(21) Zgurskaya, H. I., López, C. A., and Gnanakaran, S. (2015) Permeability Barrier of Gram-Negative Cell Envelopes and Approaches To Bypass It. *ACS Infect. Dis. 1* (11), 512−522.

(22) Murata, T., Tseng, W., Guina, T., Miller, S. I., and Nikaido, H. (2007) PhoPQ-mediated regulation produces a more robust permeability barrier in the outer membrane of Salmonella enterica serovar typhimurium. *J. Bacteriol. 189* (20), 7213−7222.

(23) CDC (2018) *CDC & FDA Antibiotic Resistance Isolate Bank,* CDC, Atlanta, GA.

(24) Wade, D., Boman, A., Wåhlin, B., Drain, C. M., Andreu, D., Boman, H. G., and Merrifield, R. B. (1990) All-D amino acid-containing channel-forming antibiotic peptides. *Proc. Natl. Acad. Sci. U. S. A. 87* (12), 4761−4765.

(25) Won, A., Khan, M., Gustin, S., Akpawu, A., Seebun, D., Avis, T. J., Leung, B. O., Hitchcock, A. P., and Ianoul, A. (2011) Investigating the effects of L- to D-amino acid substitution and deamidation on the activity and membrane interactions of antimicrobial peptide anoplin. *Biochim. Biophys. Acta, Biomembr. 1808* (6), 1592−1600.

(26) Casteels, P., and Tempst, P. (1994) Apidaecin-Type Peptide Antibiotics Function through a Nonporeforming Mechanism Involving Stereospecificity. *Biochem. Biophys. Res. Commun. 199* (1), 339−345.

(27) Bulet, P., Urge, L., Ohresser, S., Hetru, C., and Otvos, L., Jr (1996) Enlarged Scale Chemical Synthesis and Range of Activity of Drosocin, an O-Glycosylated Antibacterial Peptide of Drosophila. *Eur. J. Biochem. 238* (1), 64−69.

(28) Senn, H. M., and Thiel, W. (2009) QM/MM methods for biomolecular systems. *Angew. Chem., Int. Ed. 48* (7), 1198−1229.

(29) Vreven, T., Morokuma, K., Farkas, Ö., Schlegel, H. B., and Frisch, M. J. (2003) Geometry optimization with QM/MM, ONIOM, and other combined methods. I. Microiterations and constraints. *J. Comput. Chem. 24* (6), 760−769.
(30) Chung, L. W., Sameera, W. M. C., Ramozzi, R., Page, A. J., Hatanaka, M., Petrova, G. P., Harris, T. V., Li, X., Ke, Z., Liu, F., Li, H.-B., Ding, L., and Morokuma, K. (2015) The ONIOM Method and Its Applications. *Chem. Rev. 115* (12), 5678−5796.
(31) Chin, J. (1991) Developing artificial hydrolytic metalloenzymes by a unified mechanistic approach. *Acc. Chem. Res. 24* (5), 145−152.
(32) Bashkin, J. K., and Jenkins, L. A. (1994) The Role of Metals in the Hydrolytic Cleavage of DNA and RNA. *Comments Inorg. Chem. 16* (1−2), 77−93.
(33) Fothergill, M., Goodman, M. F., Petruska, J., and Warshel, A. (1995) Structure-Energy Analysis of the Role of Metal Ions in Phosphodiester Bond Hydrolysis by DNA Polymerase I. *J. Am. Chem. Soc. 117* (47), 11619−11627.
(34) Williams, N. H., Takasaki, B., Wall, M., and Chin, J. (1999) Structure and Nuclease Activity of Simple Dinuclear Metal Complexes: Quantitative Dissection of the Role of Metal Ions. *Acc. Chem. Res. 32* (6), 485−493.
(35) Das, P., Chandar, N. B., Chourey, S., Agarwalla, H., Ganguly, B., and Das, A. (2013) Role of Metal Ion in Specific Recognition of Pyrophosphate Ion under Physiological Conditions and Hydrolysis of the Phosphoester Linkage by Alkaline Phosphatase. *Inorg. Chem. 52* (19), 11034−11041.
(36) Prince, R. H., and Woolley, P. R. (1972) Metal Ion Function in Carbonic Anhydrase. *Angew. Chem., Int. Ed. Engl. 11* (5), 408−417.
(37) Groves, J. T., and Olson, J. R. (1985) Models of zinc-containing proteases. Rapid amide hydrolysis by an unusually acidic Zn2+-OH2 complex. *Inorg. Chem. 24* (18), 2715−2717.
(38) Nonejuie, P., Burkart, M., Pogliano, K., and Pogliano, J. (2013) Bacterial cytological profiling rapidly identifies the cellular pathways targeted by antibacterial molecules. *Proc. Natl. Acad. Sci. U. S. A. 110* (40), 16169−16174.
(39) Wu, Y., and Seyedsayamdost, M. R. (2017) Synergy and Target Promiscuity Drive Structural Divergence in Bacterial Alkylquinolone Biosynthesis. *Cell Chem. Biol. 24* (12), 1437−1444.E3.
(40) Sun, Y., Heidary, D. K., Zhang, Z., Richards, C. I., and Glazer, E. C. (2018) Bacterial Cytological Profiling Reveals the Mechanism of Action of Anticancer Metal Complexes. *Mol. Pharmaceutics 15* (8), 3404−3416.
(41) Zasloff, M. (1987) Magainins, a class of antimicrobial peptides from Xenopus skin: isolation, characterization of two active forms, and partial cDNA sequence of a precursor. *Proc. Natl. Acad. Sci. U. S. A. 84* (15), 5449−53.
(42) Ludtke, S. J., He, K., Heller, W. T., Harroun, T. A., Yang, L., and Huang, H. W. (1996) Membrane pores induced by magainin. *Biochemistry 35* (43), 13723−8.
(43) Matsuzaki, K., Murase, O., Fujii, N., and Miyajima, K. (1996) An antimicrobial peptide, magainin 2, induced rapid flip-flop of phospholipids coupled with pore formation and peptide translocation. *Biochemistry 35* (35), 11361−8.
(44) Park, C. B., Kim, M. S., and Kim, S. C. (1996) A Novel Antimicrobial Peptide fromBufo bufo gargarizans. *Biochem. Biophys. Res. Commun. 218* (1), 408−413.
(45) Park, C. B., Kim, H. S., and Kim, S. C. (1998) Mechanism of action of the antimicrobial peptide buforin II: buforin II kills microorganisms by penetrating the cell membrane and inhibiting cellular functions. *Biochem. Biophys. Res. Commun. 244* (1), 253−7.
(46) Kobayashi, S., Takeshima, K., Park, C. B., Kim, S. C., and Matsuzaki, K. (2000) Interactions of the novel antimicrobial peptide buforin 2 with lipid bilayers: proline as a translocation promoting factor. *Biochemistry 39* (29), 8648−54.
(47) Subbalakshmi, C., and Sitaram, N. (1998) Mechanism of antimicrobial action of indolicidin. *FEMS Microbiol. Lett. 160* (1), 91−6.
(48) Marchand, C., Krajewski, K., Lee, H. F., Antony, S., Johnson, A. A., Amin, R., Roller, P., Kvaratskhelia, M., and Pommier, Y. (2006) Covalent binding of the natural antimicrobial peptide indolicidin to DNA abasic sites. *Nucleic Acids Res. 34* (18), 5157−65.
(49) Yu, D., Sheng, Z., Xu, X., Li, J., Yang, H., Liu, Z., Rees, H. H., and Lai, R. (2006) A novel antimicrobial peptide from salivary glands of the hard tick, Ixodes sinensis. *Peptides 27* (1), 31−5.
(50) Libardo, M. D. J., Gorbatyuk, V. Y., and Angeles-Boza, A. M. (2016) Central Role of the Copper-Binding Motif in the Complex Mechanism of Action of Ixosin: Enhancing Oxidative Damage and Promoting Synergy with Ixosin B. *ACS Infect. Dis. 2* (1), 71−81.
(51) Hayden, R. M., Goldberg, G. K., Ferguson, B. M., Schoeneck, M. W., Libardo, M. D., Mayeux, S. E., Shrestha, A., Bogardus, K. A., Hammer, J., Pryshchep, S., Lehman, H. K., McCormick, M. L., Blazyk, J., Angeles-Boza, A. M., Fu, R., and Cotten, M. L. (2015) Complementary Effects of Host Defense Peptides Piscidin 1 and Piscidin 3 on DNA and Lipid Membranes: Biophysical Insights into Contrasting Biological Activities. *J. Phys. Chem. B 119* (49), 15235−46.
(52) Ludtke, S., He, K., and Huang, H. (1995) Membrane thinning caused by magainin 2. *Biochemistry 34* (51), 16764−9.
(53) Silver, L. L. (2011) Challenges of antibacterial discovery. *Clin. Microbiol. Rev. 24* (1), 71−109.
(54) Falla, T. J., Karunaratne, D. N., and Hancock, R. E. (1996) Mode of action of the antimicrobial peptide indolicidin. *J. Biol. Chem. 271* (32), 19298−303.
(55) Nakamura, T., Furunaka, H., Miyata, T., Tokunaga, F., Muta, T., Iwanaga, S., Niwa, M., Takao, T., and Shimonishi, Y. (1988) Tachyplesin, a class of antimicrobial peptide from the hemocytes of the horseshoe crab (Tachypleus tridentatus). Isolation and chemical structure. *J. Biol. Chem. 263* (32), 16709−16713.
(56) Matsuzaki, K., Fukui, M., Fujii, N., and Miyajima, K. (1991) Interactions of an antimicrobial peptide, tachyplesin I, with lipid membranes. *Biochim. Biophys. Acta, Biomembr. 1070* (1), 259−64.
(57) Ohta, M., Ito, H., Masuda, K., Tanaka, S., Arakawa, Y., Wacharotayankun, R., and Kato, N. (1992) Mechanisms of antibacterial action of tachyplesins and polyphemusins, a group of antimicrobial peptides isolated from horseshoe crab hemocytes. *Antimicrob. Agents Chemother. 36* (7), 1460−5.
(58) Yonezawa, A., Kuwahara, J., Fujii, N., and Sugiura, Y. (1992) Binding of tachyplesin I to DNA revealed by footprinting analysis: significant contribution of secondary structure to DNA binding and implication for biological action. *Biochemistry 31* (11), 2998−3004.
(59) Perrin, B. S., Tian, Y., Fu, R., Grant, C. V., Chekmenev, E. Y., Wieczorek, W. E., Dao, A. E., Hayden, R. M., Burzynski, C. M., Venable, R. M., Sharma, M., Opella, S. J., Pastor, R. W., and Cotten, M. L. (2014) High-Resolution Structures and Orientations of Antimicrobial Peptides Piscidin 1 and Piscidin 3 in Fluid Bilayers Reveal Tilting, Kinking, and Bilayer Immersion. *J. Am. Chem. Soc. 136* (9), 3491−3504.
(60) Libardo, M. D. J., Bahar, A. A., Ma, B., Fu, R., McCormick, L. E., Zhao, J., McCallum, S. A., Nussinov, R., Ren, D., Angeles-Boza, A. M., and Cotten, M. L. (2017) Nuclease activity gives an edge to host-defense peptide piscidin 3 over piscidin 1, rendering it more effective against persisters and biofilms. *FEBS J. 284* (21), 3662−3683.
(61) Silphaduang, U., and Noga, E. J. (2001) Peptide antibiotics in mast cells of fish. *Nature 414* (6861), 268−9.
(62) Mygind, P., Fischer, R., Schnorr, K., et al. (2005) Plectasin is a peptide antibiotic with therapeutic potential from a saprophytic fungus. *Nature 437*, 975−980.
(63) Schneider, T., Kruse, T., Wimmer, R., Wiedemann, I., Sass, V., Pag, U., Kristensen, H., et al. (2010) Plectasin, a Fungal Defensin, Targets the Bacterial Cell Wall Precursor Lipid II. *Science 328* (5982), 1168−1172.
(64) Xiang, F., Xie, Z., Feng, J., Yang, W., Cao, Z., Li, W., Chen, Z., and Wu, Y. (2015) Plectasin, first animal toxin-like fungal defensin blocking potassium channels through recognizing channel pore region. *Toxins 7* (1), 34−42.
(65) Lee, I. H., Zhao, C., Cho, Y., Harwig, S. S., Cooper, E. L., and Lehrer, R. I. (1997) Clavanins, alpha-helical antimicrobial peptides from tunicate hemocytes. *FEBS Lett. 400* (2), 158−62.

https://dx.doi.org/10.1021/acsinfecdis.0c00051
ACS Infect. Dis. 2020, 6, 1250−1263

(66) Menzel, L. P., Lee, I. H., Sjostrand, B., and Lehrer, R. I. (2002) Immunolocalization of clavanins in Styela clava hemocytes. *Dev. Comp. Immunol. 26* (6), 505−515.
(67) Wagner, D., Maser, J., Lai, B., Cai, Z., Barry, C. E., 3rd, Honer Zu Bentrup, K., Russell, D. G., and Bermudez, L. E. (2005) Elemental analysis of Mycobacterium avium-, Mycobacterium tuberculosis-, and Mycobacterium smegmatis-containing phagosomes indicates pathogen-induced microenvironments within the host cell's endosomal system. *J. Immunol. 174* (3), 1491−500.
(68) Botella, H., Peyron, P., Levillain, F., Poincloux, R., Poquet, Y., Brandli, I., Wang, C., Tailleux, L., Tilleul, S., Charrière, G. M., Waddell, S. J., Foti, M., Lugo-Villarino, G., Gao, Q., Maridonneau-Parini, I., Butcher, P. D., Castagnoli, P. R., Gicquel, B., de Chastellier, C., and Neyrolles, O. (2011) Mycobacterial p(1)-type ATPases mediate resistance to zinc poisoning in human macrophages. *Cell Host Microbe 10* (3), 248−259.
(69) Ma, L., Terwilliger, A., and Maresso, A. W. (2015) Iron and zinc exploitation during bacterial pathogenesis. *Metallomics 7* (12), 1541−54.
(70) Chandrangsu, P., Rensing, C., and Helmann, J. D. (2017) Metal homeostasis and resistance in bacteria. *Nat. Rev. Microbiol. 15* (6), 338−350.
(71) Wei, L., LaBouyer, M. A., Darling, L. E. O., and Elmore, D. E. (2016) Bacterial Spheroplasts as a Model for Visualizing Membrane Translocation of Antimicrobial Peptides. *Antimicrob. Agents Chemother. 60* (10), 6350.
(72) Wiegand, I., Hilpert, K., and Hancock, R. E. (2008) Agar and broth dilution methods to determine the minimal inhibitory concentration (MIC) of antimicrobial substances. *Nat. Protoc. 3* (2), 163−75.
(73) Vilcheze, C., Hartman, T., Weinrick, B., and Jacobs, W. R., Jr (2013) Mycobacterium tuberculosis is extraordinarily sensitive to killing by a vitamin C-induced Fenton reaction. *Nat. Commun. 4*, 1881.
(74) Silva, O. N., Alves, E. S., De La Fuente-Núñez, C., Ribeiro, S. M., Mandal, S. M., Gaspar, D., Veiga, A. S., Castanho, M. A., Andrade, C. A., Nascimento, J. M., et al. (2016) Structural studies of a lipid-binding peptide from tunicate hemocytes with anti-biofilm activity. *Sci. Rep. 6*, 27128.
(75) Krieger, E., and Vriend, G. (2014) YASARA View—molecular graphics for all devices—from smartphones to workstations. *Bioinformatics 30* (20), 2981−2982.
(76) Blattner, F. R., Plunkett, G., Bloch, C. A., Perna, N. T., Burland, V., Riley, M., Collado-Vides, J., Glasner, J. D., Rode, C. K., and Mayhew, G. F. (1997) The complete genome sequence of Escherichia coli K-12. *Science 277* (5331), 1453−1462.
(77) Hanwell, M. D., Curtis, D. E., Lonie, D. C., Vandermeersch, T., Zurek, E., and Hutchison, G. R. (2012) Avogadro: an advanced semantic chemical editor, visualization, and analysis platform. *J. Cheminf. 4* (1), 17.
(78) Yan, Y., Zhang, D., Zhou, P., Li, B., and Huang, S.-Y. (2017) HDOCK: a web server for protein−protein and protein−DNA/RNA docking based on a hybrid strategy. *Nucleic Acids Res. 45* (W1), W365−W373.
(79) Hess, B., Kutzner, C., Van Der Spoel, D., and Lindahl, E. (2008) GROMACS 4: algorithms for highly efficient, load-balanced, and scalable molecular simulation. *J. Chem. Theory Comput. 4* (3), 435−447.
(80) Vanommeslaeghe, K., Hatcher, E., Acharya, C., Kundu, S., Zhong, S., Shim, J., Darian, E., Guvench, O., Lopes, P., Vorobyov, I., et al. (2009) CHARMM general force field: A force field for drug-like molecules compatible with the CHARMM all-atom additive biological force fields. *J. Comput. Chem. 31* (4), 671−690.
(81) Duay, S. S., Sharma, G., Prabhakar, R., Angeles-Boza, A. M., and May, E. R. (2019) Molecular Dynamics Investigation into the Effect of Zinc (II) on the Structure and Membrane Interactions of the Antimicrobial Peptide Clavanin A. *J. Phys. Chem. B 123* (15), 3163−3176.
(82) Darden, T., York, D., and Pedersen, L. (1993) Particle mesh Ewald: An N· log (N) method for Ewald sums in large systems. *J. Chem. Phys. 98* (12), 10089−10092.
(83) Price, D. J., and Brooks, C. L., III (2004) A modified TIP3P water potential for simulation with Ewald summation. *J. Chem. Phys. 121* (20), 10096−10103.
(84) Miyamoto, S., and Kollman, P. A. (1992) Settle: An analytical version of the SHAKE and RATTLE algorithm for rigid water models. *J. Comput. Chem. 13* (8), 952−962.
(85) Hess, B., Bekker, H., Berendsen, H. J., and Fraaije, J. G. (1997) LINCS: a linear constraint solver for molecular simulations. *J. Comput. Chem. 18* (12), 1463−1472.
(86) Kumari, R., Kumar, R., Open Source Drug Discovery Consortium, and Lynn, A. (2014) g_mmpbsa— A GROMACS tool for high-throughput MM-PBSA calculations. *J. Chem. Inf. Model. 54* (7), 1951−1962.
(87) Frisch, M., Trucks, G., Schlegel, H., Scuseria, G., Robb, M., Cheeseman, J., Scalmani, G., Barone, V., Mennucci, B., and Petersson, G. (2009) *Gaussian 09*, rev. D.01, Gaussian, Inc., Wallingford, CT.
(88) Becke, A. D. (1988) Density-functional exchange-energy approximation with correct asymptotic behavior. *Phys. Rev. A: At., Mol., Opt. Phys. 38* (6), 3098.
(89) Hay, P. J., and Wadt, W. R. (1985) Ab initio effective core potentials for molecular calculations. Potentials for the transition metal atoms Sc to Hg. *J. Chem. Phys. 82* (1), 270−283.
(90) Wang, J., Wolf, R. M., Caldwell, J. W., Kollman, P. A., and Case, D. A. (2004) Development and testing of a general amber force field. *J. Comput. Chem. 25* (9), 1157−1174.
(91) Duan, Y., Wu, C., Chowdhury, S., Lee, M. C., Xiong, G., Zhang, W., Yang, R., Cieplak, P., Luo, R., Lee, T., et al. (2003) A point-charge force field for molecular mechanics simulations of proteins based on condensed-phase quantum mechanical calculations. *J. Comput. Chem. 24* (16), 1999−2012.
(92) Mol, A. R., Castro, M. S., and Fontes, W. (2018) NetWheels: A web application to create high quality peptide helical wheel and net projections. *BioRxiv*, 416347, .
(93) Humphrey, W., Dalke, A., and Schulten, K. (1996) VMD: visual molecular dynamics. *J. Mol. Graphics 14* (1), 33−38.
(94) Pettersen, E. F., Goddard, T. D., Huang, C. C., Couch, G. S., Greenblatt, D. M., Meng, E. C., and Ferrin, T. E. (2004) UCSF Chimera—a visualization system for exploratory research and analysis. *J. Comput. Chem. 25* (13), 1605−1612.
(95) Wu, C.-S. C., Ikeda, K., and Yang, J. T. (1981) Ordered conformation of polypeptides and proteins in acidic dodecyl sulfate solution. *Biochemistry 20* (3), 566−570.
(96) Marqusee, S., Robbins, V. H., and Baldwin, R. L. (1989) Unusually stable helix formation in short alanine-based peptides. *Proc. Natl. Acad. Sci. U. S. A. 86* (14), 5286.
(97) Mihailescu, M., Sorci, M., Seckute, J., Silin, V. I., Hammer, J., Perrin, B. S., Hernandez, J. I., Smajic, N., Shrestha, A., Bogardus, K. A., Greenwood, A. I., Fu, R., Blazyk, J., Pastor, R. W., Nicholson, L. K., Belfort, G., and Cotten, M. L. (2019) Structure and Function in Antimicrobial Piscidins: Histidine Position, Directionality of Membrane Insertion, and pH-Dependent Permeabilization. *J. Am. Chem. Soc. 141* (25), 9837−9853.
(98) McGillivray, D. J., Valincius, G., Vanderah, D. J., Febo-Ayala, W., Woodward, J. T., Heinrich, F., Kasianowicz, J. J., and Losche, M. (2007) Molecular-scale structural and functional characterization of sparsely tethered bilayer lipid membranes. *Biointerphases 2* (1), 21−33.
(99) Vanderah, D. J., Parr, T., Silin, V., Meuse, C. W., Gates, R. S., La, H., and Valincius, G. (2004) Isostructural self-assembled monolayers. 2. Methyl 1-(3-mercaptopropyl)-oligo(ethylene oxide)s. *Langmuir 20* (4), 1311−6.

https://dx.doi.org/10.1021/acsinfecdis.0c00051
ACS Infect. Dis. 2020, 6, 1250−1263